19th Brazilian Congress of Thermal Sciences and Engineering
November 6th–10th, 2022, Bento Gonçalves - RS - Brazil

ENC-2022-0132
PORE-SCALE SIMULATION OF SCALING EFFECTS ON LOSS OF PRODUCTION IN OIL RESERVOIRS

João Victor Lopes Marchiori
Rodrigo Prando Pedroni
Renato do Nascimento Siqueira
Ayrton Cavallini Zotelle
GPMF, Department of Mechanical Engineering, Instituto Federal do Espírito Santo - Campus São Mateus, Rod. BR 101 norte, km 58, Litorâneo, São Mateus - ES, 29932-540, Brazil
joaovictor.marchiori@hotmail.com
rodrigo.pedroni@hotmail.com
renatons@ifes.edu.br
ayrton.zotelle@ifes.edu.br

Fábio de Assis Ressel Pereira
Department of Industrial Technology, Universidade Federal do Espírito Santo, Avenida Fernando Ferrari, 514, Goiabeiras, Vitória - ES, 29075-910, Brazil
fabio.a.pereira@ufes.br

André Leibsohn Martins
Petrobras, Rua Horácio Macedo nº 950, Ilha do Fundão Cidade Universitária, CEP 21941-915, Rio de Janeiro -RJ, Brazil.
aleibsohn@petrobras.com.br

Abstract. *The oil is one of the biggest commodities and energy sources in the world, being crucial to diverse other industries as an input for their products, such as fuel, plastics and synthetic rubber. However, oil production involves several engineering challenges, including production losses caused by the scaling of inorganic salts throughout the reservoir, completion elements, and production column, causing problems in the extraction of the oil and financial losses. The reservoir is a porous rock that can be constituted of different materials, which has a direct influence on the scaling behavior. There are some critical parameters that influence the carbonate scaling in oil reservoirs, as the critical velocity, which depends on surface energy and Van Der Waals electromagnetic forces, surface roughness and the kinematic interaction involving the angle of impact between the grains of the porous medium and the precipitated particles of inorganic salts, such as the calcium carbonate ($CaCO_3$). This work analyze the influence of the impact angle in the scaling with a defined critical velocity, as well as its influence on the reduction of the flow rate due calcium carbonate scaling by the application of the Computational Fluid Dynamics (CFD) technique in a simplified porous medium. Numerical simulations were used to evaluate the sensibility of scaling to the critical angle of collision, which determines the preferential range that particles adhere to the surface of the porous medium grains. To evaluate this behavior, different impact angle intervals were defined as critical for the scaling to occur, from 0° to 90° with a step of 30°. The model uses a granular flow with a two-way coupling fluid-solid interaction, with the $CaCO_3$ particles represented by a Lagrangian phase with mass fraction of 2% and the fluid is water represented by an Eulerian phase. With the model and the critical parameters implemented, it was possible to verify the effects of different critical angle intervals on scaling, and consequently on the flow rate reduction. The scaling effects were modelled including a source term on momentum equation to determine the additional flow resistance due to the particles adhesion. The results show that at low velocities the collision angles tend to be small, implying a higher adhered mass than to high angles. Furthermore, the reduction in absolute permeability due to scaling generates a non-linear drop in the flow rate. Scaling has greater sensitivity to small collision angles and occurs in preferred regions.*

Keywords: *Calcium carbonate scaling, Computational Fluid Dynamics, Porous media, Flow rate, Oil reservoirs*

1. INTRODUCTION

Even though the humanity is shifting toward renewable energy sources, the oil remains one of the biggest commodities and energy sources in the world, being crucial to diverse other industries as an input for their products, such as fuel, plastics and synthetic rubber. Due to the great importance of oil in the world, technological developments and innovations in the oil sector are constantly taking place in the search to mitigate problems and improve the efficiency of the process (Schiavi and Hoffmann, 2015). Oil extraction involves many challenges, such as the scaling of inorganic salts throughout the reservoir, completion elements, and production column. During the production chain, the reservoir is the first element that can suffer the impacts of scaling and consequently lose productivity, making the companies search ways to predict and reduce its impacts.

The scaling is very present in the oil industry due the propitious thermodynamics conditions of the reservoir and the ions dissolved in the brine, resulting in the nucleation of inorganic salts, such as the calcium carbonate ($CaCO_3$). Once nucleated, these crystals may adhere to the pores of the reservoir or in the completion elements, obstructing partially or totally the passage of the oil, reducing the productivity and rising the energetic demand, or even interrupting the production. The reservoir is a porous medium and consists in many cases of sandstone, which is one of the predominant rock types in oil production (Arsalan *et al.*, 2013). The brine is responsible for keeping the Ca^{2+} and ${CO_3}^{2-}$ ions dissolved, and these ions are mainly originated from the calcite of the sandstone (Cosmo *et al.*, 2019). Normally, carbon dioxide (CO_2) is also dissolved, however pressure drop, as a result of completion elements or flows in porous media, can reduce the solubility of this gas, causing a flash of CO_2, which can unbalance the chemical reaction responsible for the formation of the inorganic salt, promoting the nucleation of calcium carbonate from the dissolved ions (Cosmo *et al.*, 2019).

Since the calcium carbonate particle has already nucleated, which means the chemical reaction has already taken place due to the favorable thermodynamic conditions, these particles may hit a solid surface and trap or reflect, depending on its kinetic parameters and properties, such as the kinetic energy and particle diameter. These and other aspects make the scaling a very complex phenomenon due to the various ways in which it can occur and the diverse factors that influence it, making the representation of all together often impractical, having to focus on a few and assess their sensitivity to the phenomenon. In the phenomenon of scaling, the velocity of the collision, the angle of the collision, the roughness of the surface, and many others parameters could have an impact on how the particle adheres or bounces on the surface.

Some parameters related to scaling have already been analyzed in previous studies, such as the critical velocity, which was studied by Thornton and Ning (1998) and defines a value of velocity below which the particles stick to the surface as a result of Van Der Waals attractive electromagnetic forces. The critical velocity is dependent on some variables, among them the interfacial energy, and it is possible to observe a great sensitivity of the critical velocity in relation to this factor. To obtain the interfacial energy and improve the representation of the phenomenon, in the present study, values of the surface energy of calcium carbonate and sandstone were extracted from experimental studies carried out by Holysz and Chibowski (1994) and Nikoo and Malayeri (2021), respectively. The Surface energy depends on a number of factors, and is treated as a portion of the Lifshitz-van Der Waals interaction and the Lewis acid-base (Holysz and Chibowski, 1994). Another relevant parameter that can be evaluated is the surface roughness, since it can influence both the wettability of the rock and the interfacial energy between the particles and the rock (Nikoo and Malayeri, 2021).

A parameter that also can influence scaling is the dynamics of particle collisions. In the dynamics of collisions, the impact angle of the particles can influence the scaling since its value affects energy dissipation caused in the process, including that dissipated by the Van Der Waals force. This means that even if the absolute velocity in two collisions are the same, the scaling behavior may be different due to the collision angle. The dynamics of collisions can be affected by the flow regime, and as shown in the work of Kececioglu and Jiang (1994), the flow in a porous medium has several different regimes and parameters for its correct characterization. This leads to the need to characterize the flow regime with dimensionless parameters that allow a description and interpretation of the phenomenon and the results according to the analyzed regime and also with the evaluated geometry.

Considering that in Thornton's formulation for the critical velocity the collision angle is not a active factor, the model does not take it into account, which could change the adhesion criterion influencing scaling, observing that the collision angle may depend on particular factors such as geometry and flow regime. Therefore, application of an angle parameter as an adhesion criterion attempts to assess what effect the angle parameter may have on scaling and on the critical velocity, since it is not known if only the critical velocity criterion represents well all collision angles.

In order to better understand the behavior and impacts of scaling, this study aims to implement the criteria of critical velocity and critical angle by Computational Fluid Dynamics (CFD) to evaluate the relationship between scaling and loss of production in oil reservoirs, making the two parameters necessary for adhesion to occur. Since the critical velocity is already a criterion applied in the analysis of scaling for turbulent flows in completion valves, such as in the work of Maciel *et al.* (2019) and also by Ferreira *et al.* (2020) which obtained results consistent with the experimental results, in this work it is intended to verify what is the scaling behavior for a Darcian flow through a simplified porous medium. Doing this sensibility study and using dimensionless parameters, the results in future works can be compared to experimental analysis to find which angle range is more accurate to have the as close as mass adherence and distribution.

2. METHODOLOGY

The geometry developed is shown in Fig. 1 and uses a simplified porous medium consisting of spherical grains in a body-centered cubic arrangement, which aims to describe a small section of the reservoir rock. Therefore, symmetry boundary conditions were applied on the side faces. The inlet and outlet sections are the two minor faces parallel located in the upper and lower, respectively, and the grain surfaces are defined with no slip condition. For the porous medium, the porosity is 0.385.

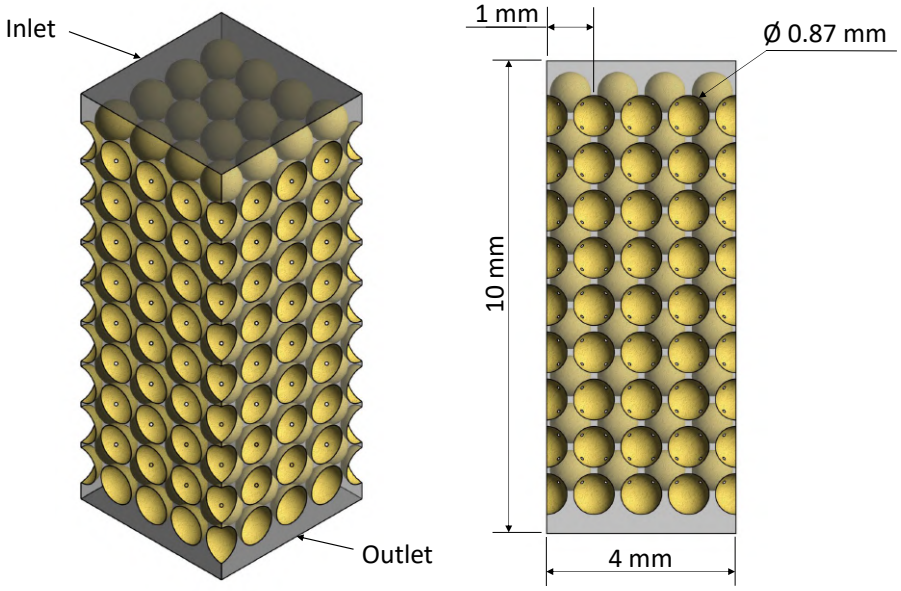

Figure 1: Simplified porous media geometry and boundary conditions.

The discrete phase model (*DPM*) was used to describe the calcium carbonate particles, injected as 2 % of the initial water mass fraction from inlet surface as previously nucleated crystals, with a diameter constant and equal to 10 μm, and density of 2800 kg/m^3. The continuos phase is the water, with density of 1000 kg/m^3 and dynamic viscosity of 0.001 $Pa.s$. A Darcian flow is assumed for the present analysis, being verified from the linearity between velocity and pressure as shown in Fig. 2, where the slope represents the initial absolute permeability of the medium $k = 4.40 \times 10^{-10}\ m^2$. Within this range where the inertial forces proved to be negligible, a pressure difference between inlet and outlet of $\Delta P = 200\ Pa$ was defined, which corresponds to a initial uniform velocity at the inlet of approximately 8.8 mm/s.

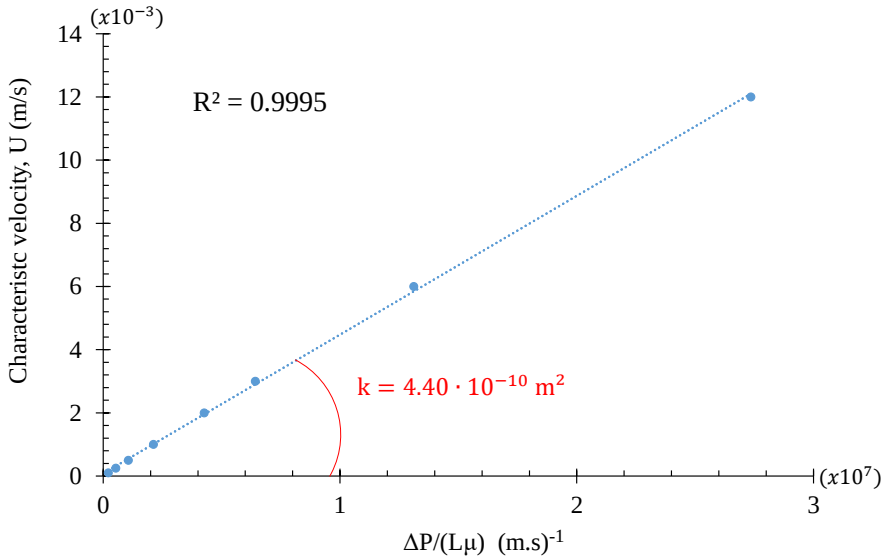

Figure 2: Darcian flow characterized by linear regression between pressure and velocity.

The representation of the surface adhesion criteria in the scaling phenomenon is defined by two critical parameters, which are the collision velocity and the impact angle. The critical velocity represents the value of velocity below which,

after the collision, the particle remains adhered to the surface due to the electromagnetic forces of Van Der Waals. The critical collision angle is defined by an interval, within which the particles also remain adhered. The addition of the critical angle allows the evaluation of the sensitivity of the scaling to the collision angle, since the critical velocity formulation does not consider it as a variable parameter. It is important to mention that both the critical velocity and the angle must be satisfied simultaneously for scaling to occur, and that surface roughness was not considered in the present study. To carry out this implementation in the physics of flow, an User Defined Function (UDF) is used to include a source term added to the momentum equation that represents the resistance caused by the packed bed of carbonate to the continuous phase.

For all simulations, the critical velocity remained constant because the formulation used is independent of the angle or variable parameters. Before carrying out the injections to analyze the scaling and the loss of production, the initial flow is considered in steady state for a Darcian flow. The cases studied had a duration of 5 seconds of simulation, with the particles being injected at the same fluid velocity during the entire flow time, with a time-step of 10^{-3} s.

In order to evaluate the sensitivity of the scaling to the collision angle, 5 cases were simulated with the general configurations described previously, in which 5 intervals of angles are stipulated so that if the particle collides within this interval and its velocity is below the critical velocity, it will stick. These cases are described in Tab. 1. The reference adopted to measure the collision angle is shown in Fig. 3, and represents the angle in relation to a tangent to the surface of the grains. It is important to note that Case 01 is taken as a reference because its angle criterion covers all possible values in a collision, which makes only the critical velocity the determining parameter in this situation. The numerical methods used to carry out the simulations are described in Tab. 2

Table 1: Range of angles for each simulated case.

Case	**Angle range for adhesion**
01	$0° < \alpha < 90°$
02	$0° < \alpha < 60°$
03	$0° < \alpha < 30°$
04	$30° < \alpha < 60°$
05	$60° < \alpha < 90°$

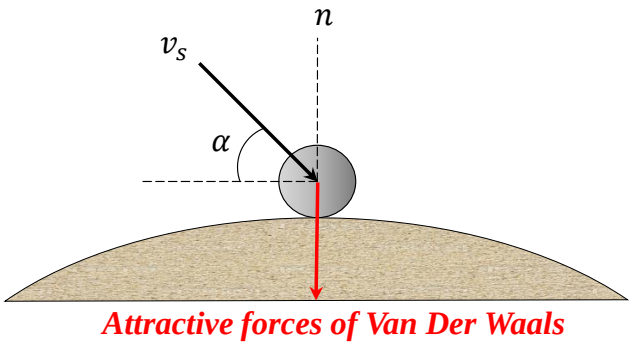

Figure 3: Reference for measuring the collision angle.

Table 2: Numerical solution methods.

Discrete phase model	Two-way coupling	
Flow regime	Darcian	
Pressure-Velocity Coupling	SIMPLE	
Spatial Discretization	Gradient	Least Squares Cell Based
	Pressure	Second Order
	Momentum	Second Order Upwind
Transient Formulation	First Order Implicit	
Time-step size	10^{-3} s	

2.1 Mathematical formulation

The mathematical modeling is described from an Euler-Lagrange approach through a two-way coupling between the discrete phase and the continuous phase, which means that the effects of one phase influence the other. For the description of the flow through the porous medium, some dimensionless parameters are used, which are:

$$\boldsymbol{u}_f^* = \frac{\boldsymbol{u}_f}{U}; \quad \nabla^* = \nabla\sqrt{k}; \quad t^* = \frac{t\mu}{\rho_f k}; \quad P^* = \frac{P}{\Delta P} \,, \tag{1}$$

where $\boldsymbol{u}_f$ is the fluid velocity vector, U is the characteristic velocity obtained by the Darcy's law $U = \frac{k}{\mu}\frac{\Delta P}{L}$, μ is the fluid viscosity, L is the length of the porous medium, k is the absolute permeability, t is the time, P is the pressure, ΔP is the pressure difference between inlet and outlet, and ρ_f is the fluid density. From the dimensionless groups above, the momentum and continuity equations were dimensionless. For the formulation of the continuous phase, the Eulerian approach is used, solving the dimensionless momentum:

$$\frac{\partial \boldsymbol{u}_f^*}{\partial t^*} + Re\ \boldsymbol{u}_f^*(\nabla^* \cdot \boldsymbol{u}_f^*) = -\nabla^* P^* + \nabla^{*2}\boldsymbol{u}_f^* + \boldsymbol{F}_{DPM}^* + \boldsymbol{F}_S^* \,, \tag{2}$$

and continuity equation for the flow field:

$$\nabla^* \cdot \boldsymbol{u}_f^* = 0 \,. \tag{3}$$

$\boldsymbol{F}_{DPM}^*$ is the source term due to interaction with the discrete phase, $\boldsymbol{F}_S^*$ is the source term due to carbonate bed scaling, and Re is the Reynolds number defined by:

$$Re = \frac{\rho_f U\sqrt{k}}{\mu} = \frac{\rho_f \Delta P k^{3/2}}{L\mu^2} \,, \tag{4}$$

in which the characteristic length is used in this study as the square root of permeability (Kececioglu and Jiang, 1994). This results on a number of Reynolds of $Re = 0.185$, showing that the advective/inertial term of the dimensionless momentum equation is negligible. For the discrete phase, the Lagrangian approach is used by the discrete phase model (DPM), tracking each particle individually through Newton's second law:

$$m_p \frac{d\boldsymbol{u}_p}{dt} = \frac{1}{2}\rho_f C_D A|\boldsymbol{u_f} - \boldsymbol{u}_p|(\boldsymbol{u_f} - \boldsymbol{u}_p) \,, \tag{5}$$

in which $m_p = \rho_p \pi d_p^3/6$ is the particle mass, $A = \pi d_p^2/4$ represents the surface area, where d_p is the particle diameter and ρ_p is the particle density. The drag coefficient is $C_D = 24/Re_p$, with $Re_p = \rho_f d_p|\boldsymbol{u_p} - \boldsymbol{u_f}|/\mu$ and $\boldsymbol{u_p}$ is the particle velocity vector. For the implementation of the scaling phenomenon, the source term is written and passed to the solver from the UDF, which introduces, through the inclusion of a local permeability, a resistance of an scaled packed bed to flow in domain cells that have scaling, calculated by:

$$\boldsymbol{F}_S{}^* = \frac{V_p}{V_c\beta^2\left(1-\frac{V_p}{V_c}\right)^3}\frac{\sqrt{k}}{\Delta P}\left(150\frac{V_p}{V_c}\mu\boldsymbol{u_f} + 1.75\beta\rho_f|\boldsymbol{u_f}|\boldsymbol{u_f}\right) \,, \tag{6}$$

where:

$$\beta = \frac{V_p}{V_c\ 0.64}d_p + \left(1 - \frac{V_p}{V_c\ 0.64}\right)^{4/3} V_c{}^{1/3} \,. \tag{7}$$

In which V_p is the volume of particles that adhere to the numerical cell adjacent to the impact surface, V_c is the volume of the numerical cell evaluated. The critical velocity represents the velocity below which the particle does not have enough kinetic energy to overcome Van Der Waals forces and reflect, remaining adhered to the surface, and is expressed by:

$$v_s = 1.84\left[\frac{32(\Gamma/d_p)^5}{\rho_p^3 E^{*2}}\right]^{1/6} \,, \tag{8}$$

where the particle diameter is constant and equal to 10 μm for all cases, the particle density is 2800 kg/m^3, and $\Gamma = 1.02 \times 10^{-3}\ J/m^2$ is the interface energy between carbonate and sandstone, determined from the surface energy of each component. The reduced Young modulus (E^*) is:

$$E^* = \left[\frac{(1-\nu_1^2)}{E_1} + \frac{(1-\nu_2^2)}{E_2}\right]^{-1} \,, \tag{9}$$

in which $E_1 = 35\ GPa$ and $E_2 = 36.4\ GPa$ are the Young modulus of calcium carbonate and sandstone, respectively, and ν_1 and ν_2 are the Poisson coefficient of calcium carbonate and sandstone, respectively, which corresponds to 0.27 for both (Xu *et al.*, 2016; Ferreira *et al.*, 2020). From these values, the critical velocity is $1.09\ mm/s$ for all cases evaluated. In case the particles do not comply with the adhesion criteria to trap, they will be reflected with a tangential restitution coefficient $e_t = 0.9$ and normal restitution coefficient e_n:

$$e_n = \left[1 - \left(\frac{v_s}{v_i}\right)^2\right]^{1/2} . \tag{10}$$

3. RESULTS AND DISCUSSIONS

3.1 Grid Independence test

The mesh test was carried out evaluating the variation of the pressure difference between inlet and outlet in steady state without particles for 7 different meshes, maintaining the same velocity of $1\ mm/s$. The mesh refinement was carried out until the pressure difference value was asymptotized and was satisfactorily independent of the mesh as show Fig. 4. In the absence of experimental data, the most refined mesh with the asymptotic tendency was assumed as the reference, and from that a tolerance of $2\ \%$ was stipulated in relation to this pressure, thus choosing Mesh 05 with 5.9 Millions of nodes (Fig. 5). Furthermore, the independence of the mesh regarding scaling was also verified in a transient regime, observing a difference of adhered mass between Mesh 07 and Mesh 05 of less than $2\ \%$.

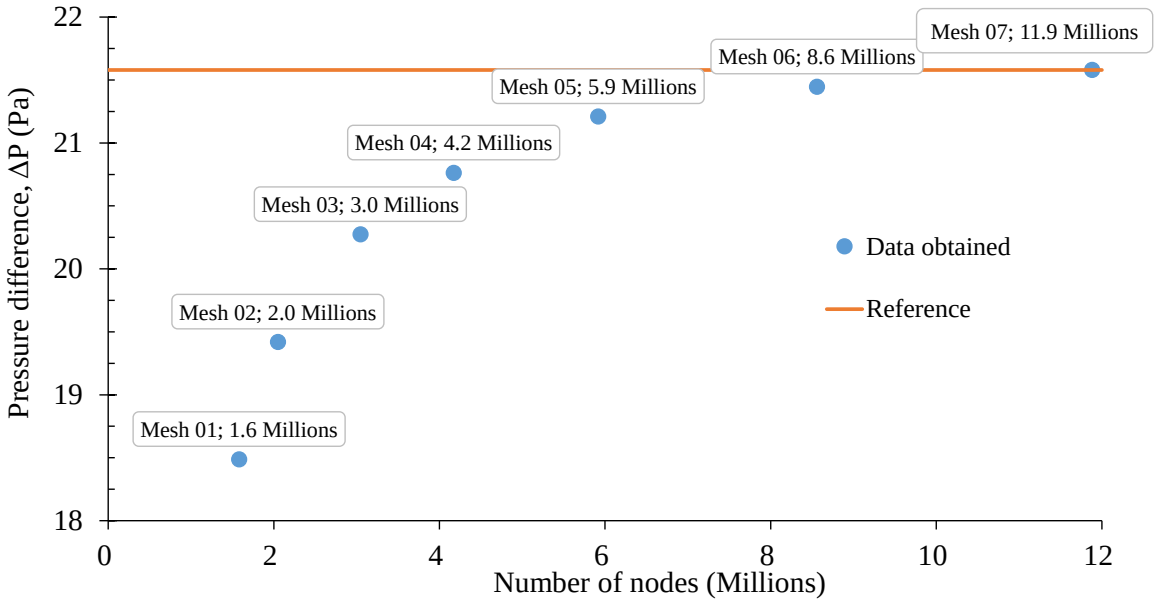

Figure 4: Mesh independence test.

3.2 Numerical simulation results

The dimensionless total mass adhered at the final volume porous injected is shown in the Fig. 6, in which the volume porous injected (V_{PI}) represents the dimensionless time. Mathematically, the V_{PI} expresses the volume of water injected until a given instant of time in relation to the total porous volume of the medium. As expected, the interval that considers the critical angle between 0° and 90° obtained the highest scaling, since for this case any angle that the particle colliding with the surface will cause it to stick, considering that the velocity is below the critical. However when compared to cases 0° to 30° and 0° to 60°, is observed a very small difference in adhered mass, which indicates that most particles tend to collide when below the critical velocity at low angles, mainly 0° and 30°.

Another fact still analyzing the Fig. 6 is that there is a low adhered mass of cases 04 and 05, which means that even if the particles are reflected at low angles and suffer a reduction in velocity due to the restitution, they do not tend to scale with collision at high angles. This means that if low collision angles are critical for adhesion, scaling will be more pronounced, such as in Case 03. However, if high angles such as Case 04 and Case 05 are more representative for adhesion, the sensitivity of the scaling to the angle is small as will be explained later in this work.

To evaluate the behavior at smaller ranges of angles for the cases 01, 02 and 03, Fig. 7 and Fig. 8 show the percentage adhered to the range in relation to the total trapped/scaled, in which it is observed that the distribution is very similar for the

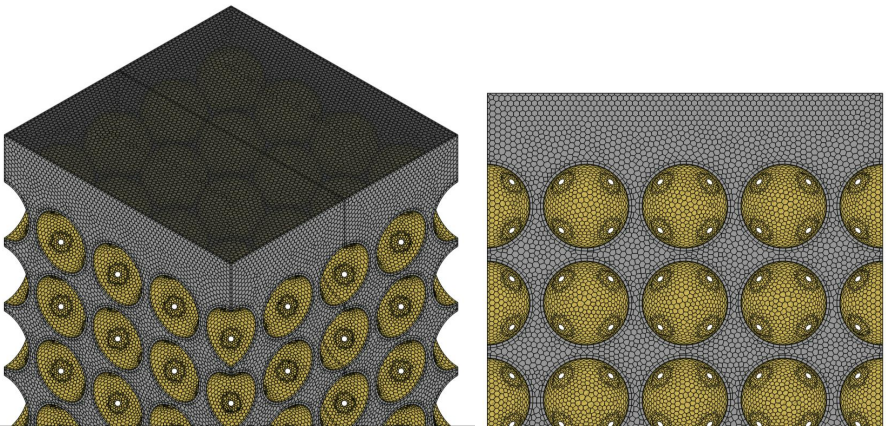

Figure 5: Mesh 05 selected for the simulations.

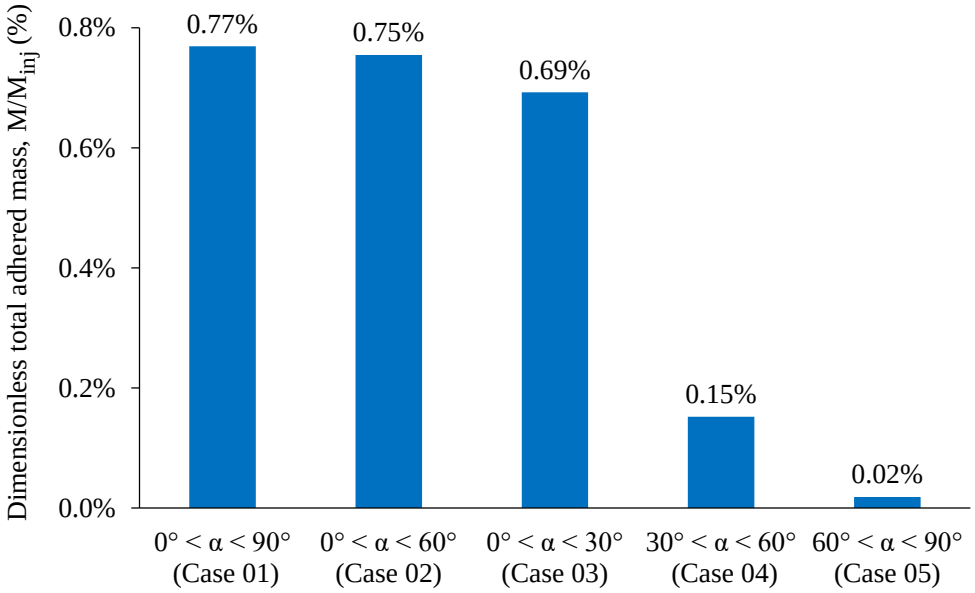

Figure 6: Dimensionless total mass adhered $M_{dim} = M/M_{inj}$ at the final instant of the simulation ($t = 5\ s$ or $V_{PI} = 11.42$). In which $V_{PI} = Q_i t/V_P$, where Q_i is the initial flow rate and V_P is the total porous volume of the medium. M is the adhered mass and M_{inj} is the total mass injected.

three cases, agreeing with what was discussed previously due to the tendency of collisions to concentrate at small angles. Analyzing the distribution better, it is possible to notice that in fact the preferred collision angles that cause adhesion are even smaller than 30°, with the highest percentage remaining below 20°, showing that collisions occur mostly at very small angles and that most of the particles adhere between 10° and 15° for the three cases.

For a visual representation of this discussion, Fig. 9 shows the distribution of the adhered mass along the surface of the porous medium at the inlet and outlet for 0º to 30º case at the final simulation time. There is a great tendency for particles to adhere to the first grains of the medium, which indicates that in this region, besides to the velocity being low enough to satisfying the critical velocity criterion, the flow allowed low collision angles. The lowest inlet velocity occurs due to the area at the inlet be larger than the area available in the region between the grains. However, when Case 01 that allows particle adhesion also at high angles is evaluated from Fig. 10, the visual aspect is very similar to that of Case 03 of Fig. 9, and this observation reinforces the fact that the range from 0º to 30º is the most significant. With this, it is possible to observe that the Darcian flow did not allow the particles to have inertia enough for the shock to occur for larger angles, causing the particles to be almost always carried along the streamlines. This causes many particles to follow without adhering inside the porous medium, until they reach the outlet. This result could be different if the flow regime had significant inertia.

A similar behavior was observed in the outlet region of the porous medium for both cases, where there is again a tendency to scaling, now in the region of the last throat between the grains before reaching the outlet. This is because,

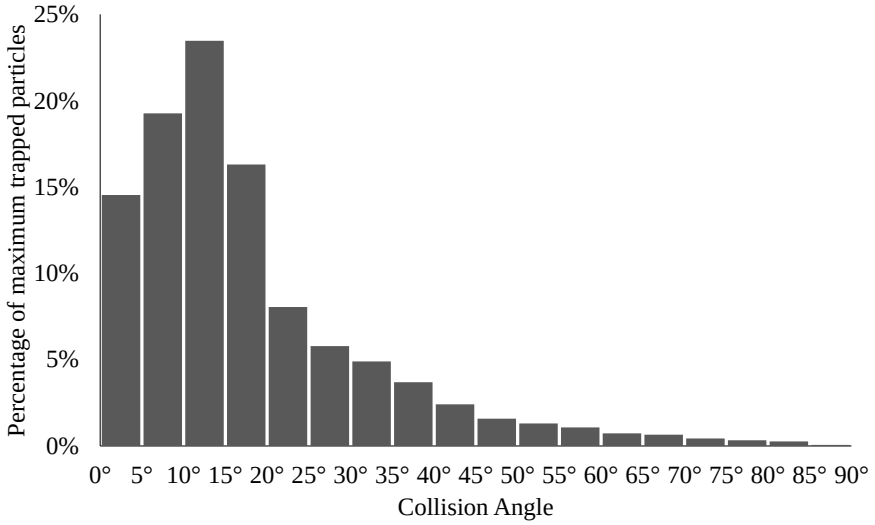

Figure 7: Distribution of trapped particle collision angle for 0º to 90° (Case 01) at $V_{PI} = 11.42$.

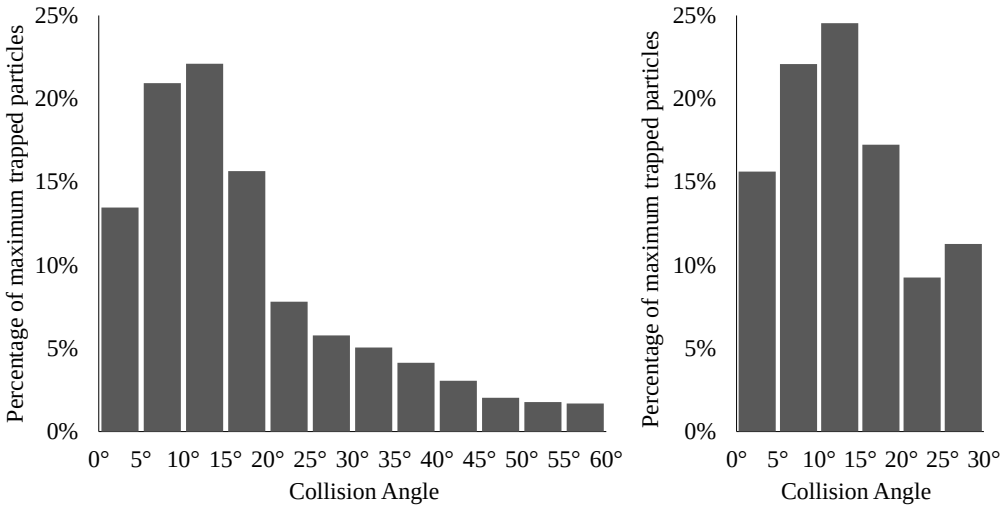

Figure 8: Distribution of trapped particle collision angle for 0° to 60° (Case 02) and for 0° to 30° (Case 03) at $V_{PI} = 11.42$.

besides to the collision at low angles caused in this Darcian regime, the velocity drops significantly in this region due to the increase in area that occurs at the end of the porous medium, and this allows the particle velocity to be lower than the critical velocity. Figure 11 shows that Case 05 had a very different behavior in relation to scaling, showing that in fact the particles do not tend to collide at high angles, although also obtained a certain tendency of scaling at the inlet and outlet of the domain. However, in all cases there is little scaling in the innermost region of the porous medium, which can be explained by Fig. 12 which shows the high velocities of $80\ mm/s$ reached in the regions of the throats between the grains, caused by the acceleration due to the reduction of area, being higher than the critical velocity and not allowing adhesion, even if the collision angle is within the criterion.

The velocity field of Fig. 12 shows the preferential scaling at the inlet and outlet of the porous medium for Case 03 at the final instant, where it is possible to observe the reason why this occurs. In the inlet region, there are low velocities in the upper region of the grains, which permit scaling. At the outlet, the flow is decelerated, which again allows a particle velocity below the critical, causing scaling. In addition to the low velocities, the collision angles are low due to the small inertia of the particles, which causes them to follow the well-defined streamlines in the Darcian regime, colliding at low angles. This characteristic of streamlines allows us to observe that many particles leave the domain without colliding with the grain surface. This observation corroborates the low scaling analyzed in the internal region of the porous medium.

It is possible to verify that the scaled regions that are highlighted in Fig. 12 show the tendency of the fluid to bypass these places, since they cause greater resistance to flow. The scaling between the throats at the outlet caused by the reduction in velocity forces the flow to pass through the center, generating a local acceleration and increasing the head loss that implies a reduction in production flow rate, since the pressure difference between inlet and outlet is constant. This shows that it would take more energy to maintain the same production through the porous medium. The scaling developed

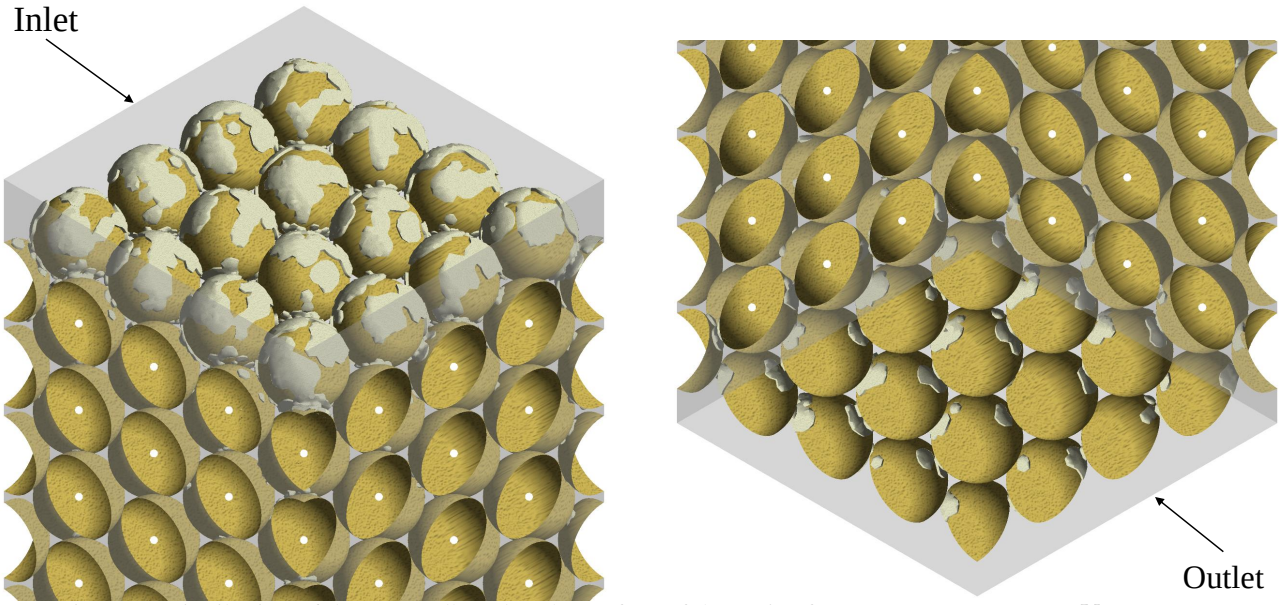

Figure 9: Distribution of the mass adhered to the surface of the grains for 0° to 30° (Case 03) at $V_{PI} = 11.42$.

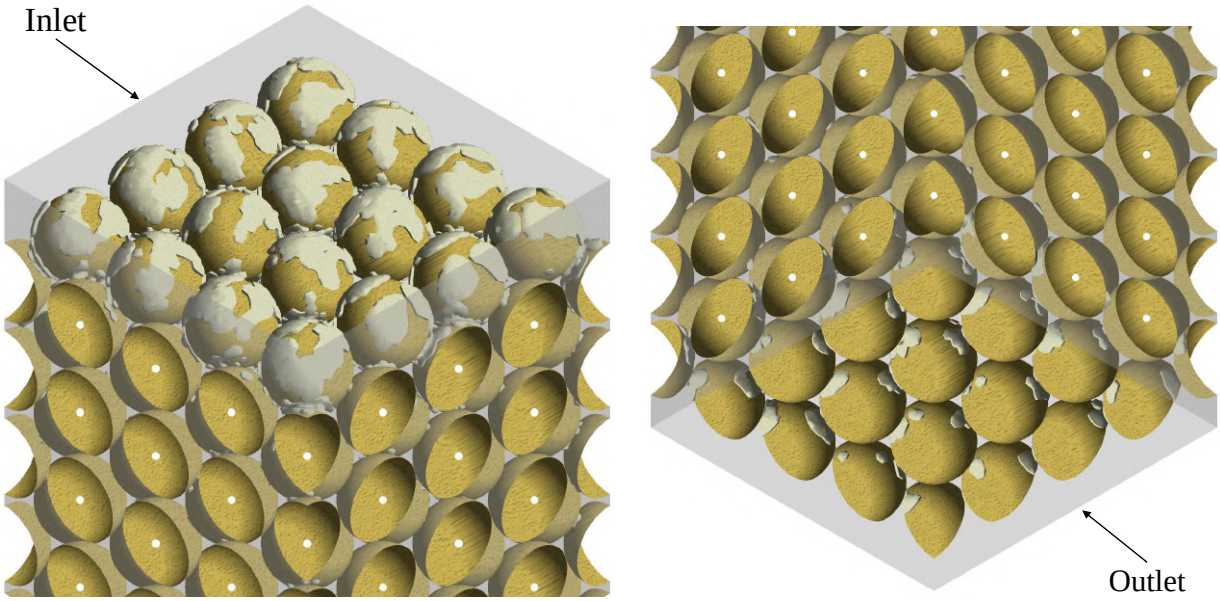

Figure 10: Distribution of the mass adhered to the surface of the grains for 0° to 90° (Case 01) at $V_{PI} = 11.42$.

in the inlet grains also generate resistance to flow, and occur preferentially in the upper region of these grains. It is also observed that dead zones are created in the vertical space between two grains.

In order to evaluate any tendency in the behavior of the scaling rate, the dimensionless scaling rate over V_{PI} can be evaluated by Fig. 13, which is represented by the moving average (for each 150 time-step) of the percentage rate at which the mass adheres to the surface of the porous medium in relation to the injected mass flow rate of particles. Figure 13a shows the behavior for cases 01, 02 and 03, where it is observed that the scaling rates are also similar due to the collision tendency at small angles. The initial transient behavior is observed in all three cases, as well as a tendency towards rate stabilization from $V_{PI} = 2$ onwards, although the behavior is still very oscillatory to be considered in steady state.

Figure 13b illustrates the cases 03, 04 and 05 that cover 3 independent intervals of angles, since they do not have common angles. The behavior of the scaling rate was very different, with Case 03 showing a much higher scaling rate than the others. The Fig. 13b also reveals by the cases 04 and 05 (since only independent intervals are compared) that again there is low scaling sensitivity for high angles but high sensitivity for low angles. The average scaling rate between V_{PI} from 2 to 11.42 for the simulated cases are summarized in Tab. 3.

In order to analyze the effect that the resistance generated by the scaling has on the scaling itself due to the change in the velocity field, Fig. 14 shows the scaling rate over V_{PI} for the case from 0º to 30º denoted No Resistance (NR) with the

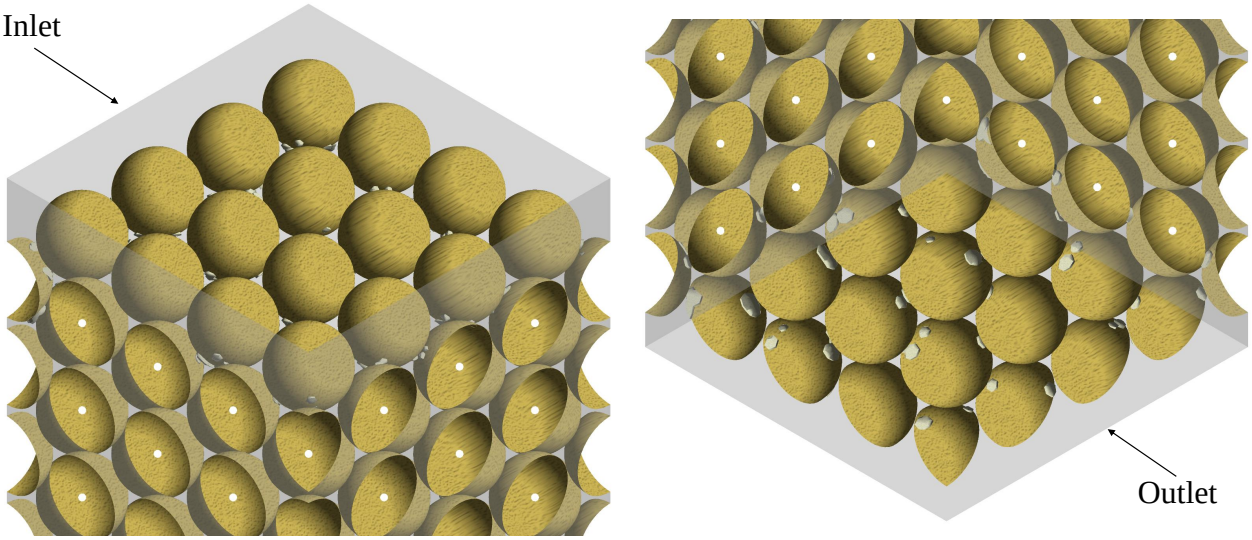

Figure 11: Distribution of the mass adhered to the surface of the grains for 60° to 90° (Case 05) at $V_{PI} = 11.42$.

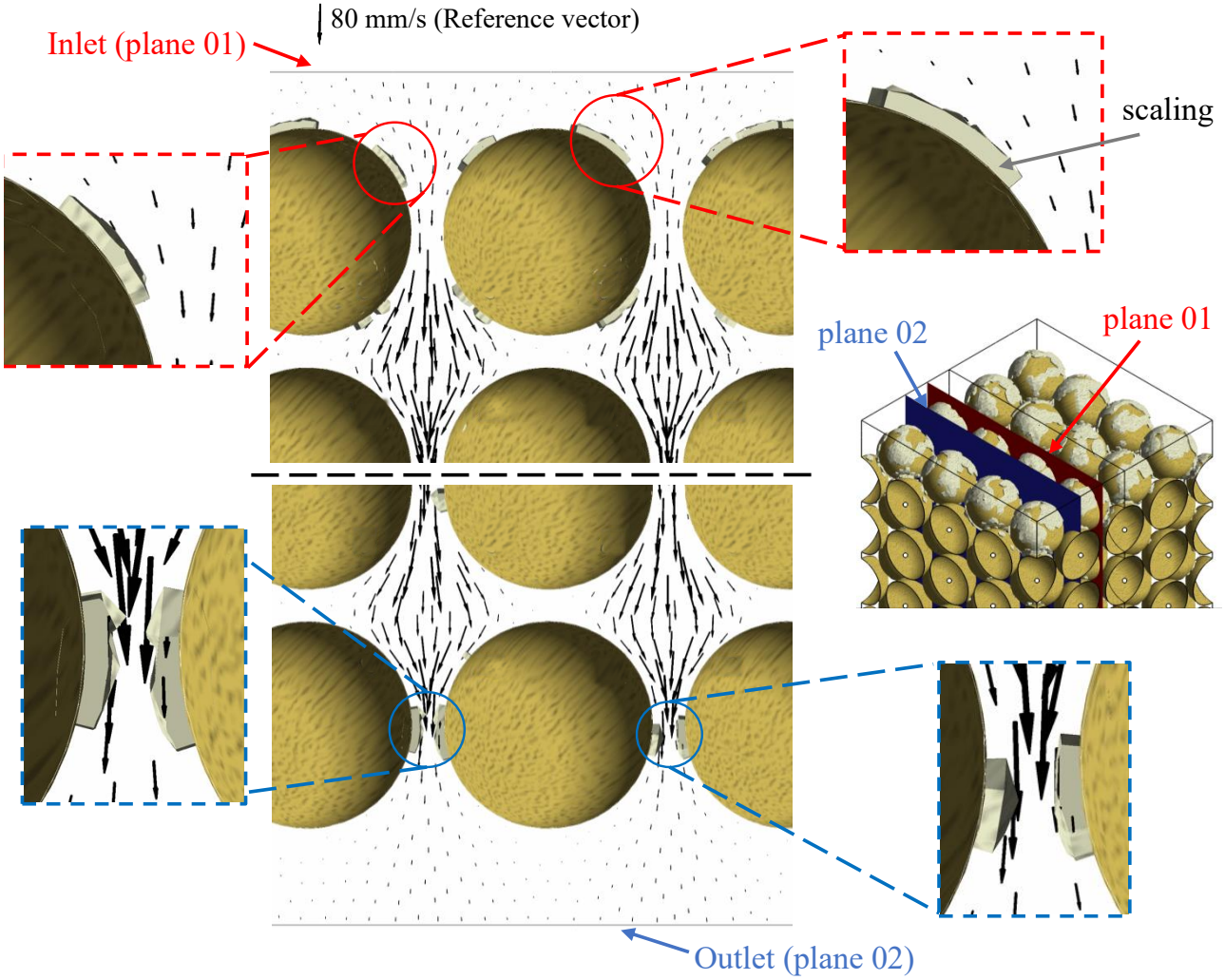

Figure 12: Velocity vectors at the inlet and outlet of the domain for 0° to 30° case at $V_{PI} = 11.42$.

governing equations without the source of resistance term and the Case 03 already shown and which has the resistance. It is verified that the case with resistance (Case 03) has a lower rate of adhesion of the particles, which can be explained by the fact that the decrease in absolute permeability close to the walls makes the flow field tend to bypass this region and

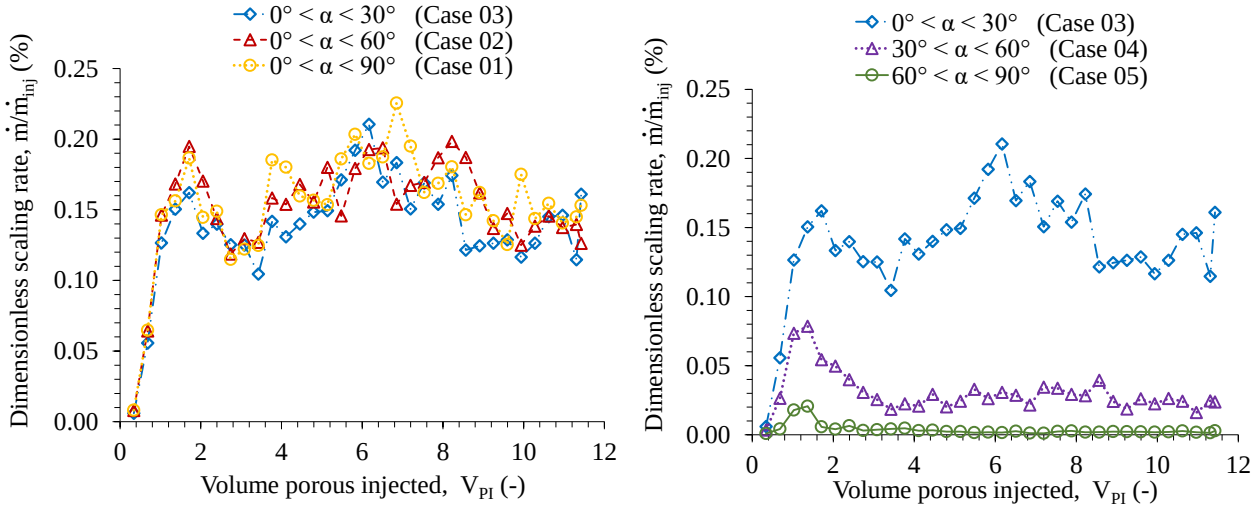

(a) (b)

Figure 13: Dimensionless scaling rate $\dot{m}_{dim} = \dot{m}/\dot{m}_{inj}$ over V_{PI}. In which $\dot{m}$ is the adhered mass rate and $\dot{m}_{inj}$ the mass flow rate of particles injected. (a) cases 01, 02 and 03 and (b) cases 03, 04 and 05.

Table 3: Average scaling rate for $2 < V_{PI} < 11.42$.

Case	Average scaling rate
01	0.161 %
02	0.156 %
03	0.146 %
04	0.027 %
05	0.003 %

follow the grain throats, since this path offers the least resistance, and this makes the particles collide less with the surface. This behavior can be seen in Fig. 12, where the flow tends to avoid the scaling regions. Furthermore, as a side effect, the additional acceleration generated by the reduction in area due to scaling in the porous media throats makes it more difficult for the particle to reach low velocities. On the other hand, when scaling does not cause flow resistance, the scaling rate is higher, as shown in the case 0º to 30º without resistance. This means that for the flow resistance modeled by adding a local permeability, the scaling mitigates the formation of new scaling.

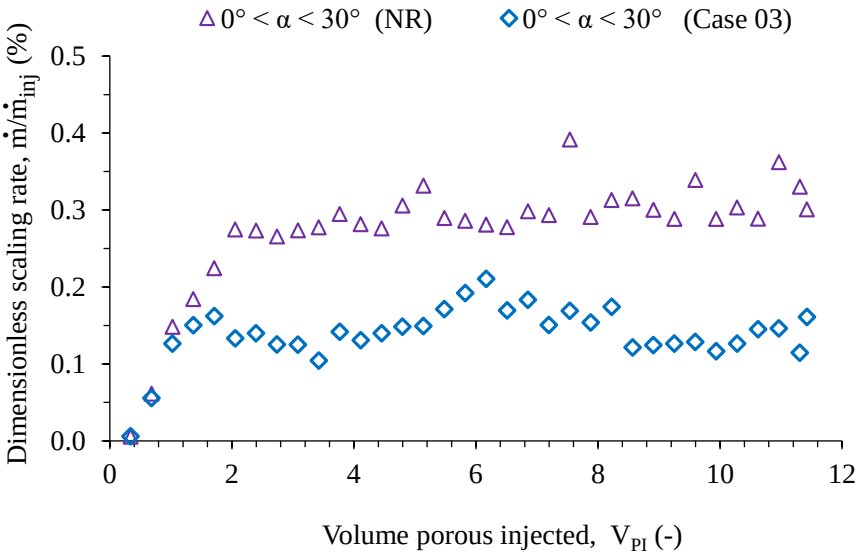

Figure 14: Dimensionless scaling rate $\dot{m}_{dim} = \dot{m}/\dot{m}_{inj}$ over V_{PI}. In which $\dot{m}$ is the adhered mass rate and $\dot{m}_{inj}$ the mass flow rate of particles injected.

To evaluate the loss in productivity of the porous medium, a dimensionless flow rate as a function of V_{PI} are shown in Fig. 15. It is important to mention that the values of the graph represents only time instants after the $V_{PI} = 2$ so that the scaling behavior after the initial transient regime can be evaluated. From the data on scaling for each case as shown, the Fig. 15 shows the behavior of the flow rate drop consistent with the adhered mass and scaling rate, that is, the greatest drops in productivity occur for the cases that have more scaling. The cases of greater adherence, such as cases 01, 02 and 03, showed a similar rate of drop in flow rate, while Case 05 had a very small rate and Case 04 was shown to be intermediate. For Case 03, the dimensionless flow rate in the final $V_{PI} = 11.42$ is approximately $99.85\ \%$ of the initial flow rate, which means that, since a production pressure difference is held constant and Darcy's law applies to flow with negligible inertia, both the flow rate and the absolute permeability of the medium are reduced by about $0.15\ \%$ due to the scaling, representing a significant production loss since the total simulation time is only 5 seconds. To compare the values between the simulated cases, Tab. 4 summarizes the flow reduction and absolute permeability for all cases, for the final simulation time.

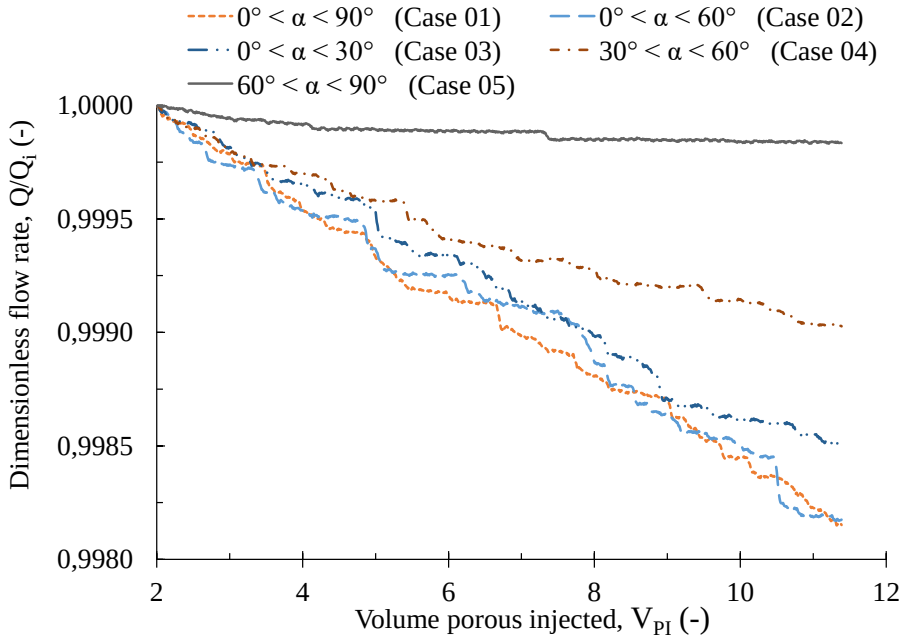

Figure 15: Dimensionless flow rate drop $Q_{dim} = Q/Q_i$ over V_{PI} for the simulated cases. In which Q is the flow rate and Q_i is the initial flow rate.

Table 4: Reduction of flow rate and absolute permeability for $V_{PI} = 11.42$.

Case	**Reduction of flow rate and absolute permeability**
01	0.185 %
02	0.183 %
03	0.149 %
04	0.097 %
05	0.017 %

4. CONCLUSION

For a Darcian flow regime the collisions and consequently the scaling tend to be more pronounced if small angles are critical, causing larger permanent productivity losses due to the reduction in the absolute permeability of the medium. To maintain the same flow and productivity, it would be necessary to supply more energy, considering that the reservoir is already operating at its maximum capacity, which can generate additional costs for oil extraction through the use of recovery methods. The scaling showed preferential regions to occur in the geometry, which are located in the first spheres of the inlet and in the last ones before the outlet, although it also occurs in a reduced way inside the porous medium. This means that scaling tends to be more significant whenever there is a transition in the geometry that causes lower velocities. For further analyses, the inclusion of other critical parameters besides velocity and angle as well as the inclusion of a multiphase water-oil flow or the roughness of the surface can improve the representation of oil extraction.

5. ACKNOWLEDGEMENTS

The authors would like to thanks Petrobras for the financial support and Instituto Federal do Espírito Santo campus São Mateus for the structure to the development of this research .

6. REFERENCES

Arsalan, N., Palayangoda, S.S., Burnett, D.J., Buiting, J.J. and Nguyen, Q.P., 2013. "Surface energy characterization of sandstone rocks". *Journal of Physics and Chemistry of Solids*, Vol. 74, No. 8, pp. 1069–1077. doi:10.1016/j.jpcs.2013.02.027.

Cosmo, R.P., Pereira, F.A.R., Ribeiro, D.C., Barros, W.Q. and Martins, A.L., 2019. "Estimating CO2 degassing effect on CaCO3 precipitation under oil well conditions". *Journal of Petroleum Science and Engineering*, Vol. 181, p. 106207. doi:10.1016/j.petrol.2019.106207.

Ferreira, M.V.D., Martins, A.L., Maciel, R.S., Fejoli, R.F., Pereira, F.R., Poletto, V.G., Lai, F.C.D. and Junqueira, S.L.D.M., 2020. "New scale prediction approach through numerical simulations". In *Day 4 Thu, October 29, 2020*. SPE. doi:10.2118/201524-ms.

Holysz, L. and Chibowski, E., 1994. "Surface free energy components of calcium carbonate and their changes due to radiofrequency electric field treatment". *Journal of Colloid and Interface Science*, Vol. 164, No. 1, pp. 245–251. doi:10.1006/jcis.1994.1163.

Kececioglu, I. and Jiang, Y., 1994. "Flow through porous media of packed spheres saturated with water". *Journal of Fluids Engineering*, Vol. 116, No. 1, pp. 164–170. doi:10.1115/1.2910229.

Maciel, R.S., Pereira, F.A.R., Ribeiro, D.C., Martins, A.L. and Ferreira, M.V.D., 2019. "Modelagem da incrustação de cristais de carbonato de cálcio nas superfícies internas de válvulas de completação pela técnica de cfd". SPE.

Nikoo, A.H. and Malayeri, M.R., 2021. "On the affinity of carbonate and sandstone reservoir rocks to scale formation – impact of rock roughness". *Colloids and Surfaces A: Physicochemical and Engineering Aspects*, Vol. 610, p. 125699. doi:10.1016/j.colsurfa.2020.125699.

Schiavi, M.T. and Hoffmann, W.A.M., 2015. "Cenário petrolífero: sua evolução, principais produtores e tecnologias". *RDBCI: Revista Digital de Biblioteconomia e Ciência da Informação*, Vol. 13, No. 2, p. 259. doi:10.20396/rdbci.v13i2.2104. URL `https://doi.org/10.20396/rdbci.v13i2.2104`.

Thornton, C. and Ning, Z., 1998. "A theoretical model for the stick/bounce behaviour of adhesive, elastic-plastic spheres". *Powder Technology*, Vol. 99, No. 2, pp. 154–162. doi:10.1016/s0032-5910(98)00099-0.

Xu, H., Zhou, W., Xie, R., Da, L., Xiao, C., Shan, Y. and Zhang, H., 2016. "Characterization of rock mechanical properties using lab tests and numerical interpretation model of well logs". *Mathematical Problems in Engineering*, Vol. 2016, pp. 1–13. doi:10.1155/2016/5967159. URL `https://doi.org/10.1155/2016/5967159`.

7. RESPONSIBILITY NOTICE

The authors are solely responsible for the printed material included in this paper.